A Classification Scheme of Natural Radiation Stain Morphology and Texture on Diamond

Taryn Linzmeyer, Roy Bassoo, Sally Eaton-Magaña, Bernd Zechmann, Nathan D. Renfro, and John I. Koivula

Although green surface coloration on diamonds is mentioned in numerous studies, no morphological classification of the subject appears to exist. This study presents a classification of radiation stain morphology and texture to supplement known characteristics of naturally irradiated diamonds. "Radiation stains," as they are often termed by gemologists, are a common indicator of alpha radiation damage that can impart a green color, which may turn brown with annealing. Studying radiation stain micromorphology and textural characteristics informs us of diamond residence in sedimentary systems, which helps to better characterize green diamonds. In this study, 84 natural diamonds with radiation stains were cataloged using photomicrography. Additionally, four of these were cataloged using atomic force microscopy. These stains were classified by color, opacity, shape, and coincident surface textures. For this study, green and brown radiation stains covered up to 93% and 12% of the diamond surface, respectively. Shapes were regular (circular or oval-shaped) or irregular and formed isolated or nondiscrete color zones. In regions imaged, circular radiation stains ranged in diameter from 22–77 μm, and oval-shaped ones ranged from 25–104 μm at their short axis to 36–158 μm at their long axis as viewed on their surface plane. One diamond exhibited raised surface topography coincident with radiation staining, and two had staining accompanying ruts or cracks. In 24% of the diamonds, the rare occurrence of fine negative surface topography coincident with radiation stains was documented. These features were angular to rounded, and some had acicular to tabular habits. The cause of the textural complexity coincident with radiation stains is currently a subject of debate and in some cases may involve localized diamond dissolution in the near-surface environment.

Diamonds residing in placer deposits frequently display distinct patches of green and/or brown coloration due to radiation damage from nearby radioactive minerals or fluids. These zones of color, termed "radiation stains" by gemologists, form from alpha (α) radiation exposure, which damages the crystal structure, creating vacancies and interstitials (Raal and Robinson, 1980; Koptil and Zinchuk, 2000; Breeding et al., 2018) (figure 1). Radiation damage leads to the formation of the GR1 defect (V^0, ZPL 741 nm), which primarily absorbs light in the red region of the visible spectrum (Clark et al., 1956). In type I diamonds with green bodycolor, absorption in the blue portion of the visible spectrum is often caused at least in part by nitrogen-related centers (e.g., Collins, 1982; Green et al., 2022). In radiation stains themselves, the stains can appear as green even in the absence of significant nitrogen content. For example, green radiation stains are observed on type II diamonds, even those with blue bodycolor (e.g., figure 15 in Eaton-Magaña et al., 2018).

Green stains can turn brown due to natural or laboratory annealing, or accidental and uncontrolled heat during polishing. This is due to annihilation of the GR1 defect and the depletion of the corresponding red absorption (e.g., Nasdala et al., 2013; Eaton-Magaña and Moe, 2016; Eaton-Magaña et al., 2023).

Green diamonds primarily colored by the GR1 can occur in kimberlites (e.g., Vance et al., 1973), but they are more prevalent in ancient diamondiferous paleoplacer or sedimentary rocks, which can have abundant radioactive minerals such as zircon,

See end of article for About the Authors and Acknowledgments.

Gems & Gemology, Vol. 62, No. 1, pp. 4–24,
https://doi.org/10.5741/GEMS.62.1.4

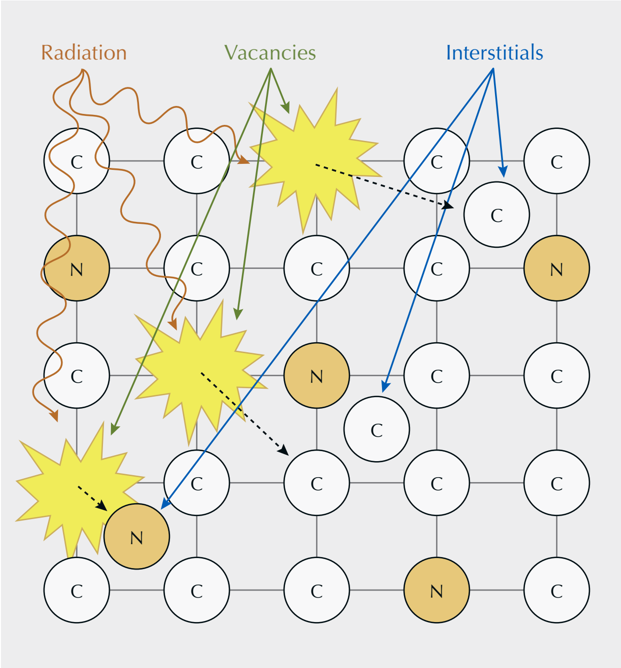

Figure 1. Schematic representation of radiation damage creating vacancies and interstitials (atoms displaced from their positions) within the diamond structure. The circles labeled "C" represent carbon atoms, and the circles labeled "N" represent nitrogen atoms.

monazite, uraninite, and thorianite. They are most commonly found in Brazil, Guyana, Venezuela, Zimbabwe, the Central African Republic, and India (Breeding et al., 2018). One major source of green diamonds, the Roraima Supergroup in South America, is host to ancient diamondiferous sedimentary rocks that are >1.75 billion years old (Santos et al., 2003; Beyer et al., 2015). Prolonged burial provides ample time and opportunity for continuous irradiation (Chaves et al., 2001; Santos et al., 2003; Schulze and Nasdala, 2016).

The type of radiation influences the intensity and depth of green color penetration in the diamond.

In Brief

- Radiation stains on diamond can be brown or green and form isolated or nondiscrete shapes.
- Shallow negative surface textures coincident with radiation stains may indicate diamond etching following irradiation in the near-surface environment.
- Radiation stains on diamond can be classified based on color, opacity, shape, and coincident features.

Alpha radiation results in the shallowest penetration, with damage to diamond confined to depths within 25–30 μm (Nasdala et al., 2013; Breeding et al., 2018; Eaton-Magaña et al., 2018). When present, radiation stains are often located on the surface of diamonds and may exhibit strain when viewed in cross-polarized light (Koivula, 2000). They also can occur internally in etch channels (figure 2), or rarely as halos of green color observed around radioactive inclusions (Koivula, 2000).

Naturally green diamonds are of particular interest to the trade due to their value and rarity. Fancy-color diamonds are uncommon, with those having natural green, blue, or pink/red color components accounting for about 0.4% of all diamonds submitted to GIA (Breeding et al., 2018).

During manufacturing, diamond polishers can preserve natural green radiation stains on the girdle or pavilion to allow perceived green color through the table, thereby adding value to an otherwise colorless diamond (Koivula, 2000; Breeding et al., 2018). Documenting the characteristics of natural green diamonds, especially those of known provenance, provides a baseline for future comparison with diamonds irradiated in a laboratory setting. In this study, photomicrography of natural diamonds permits the development of a radiation stain classification scheme based on observations of green and/or brown radiation stain morphology and associated textures for use in the gem trade.

Figure 2. This faceted diamond with etch channels shows a number of radiation stain halos resulting from shallow alpha radiation that extend along its length. The etch channels and radiation stains on the original natural surface were retained after faceting. Photomicrograph by Nathan Renfro; field of view 1.03 mm.

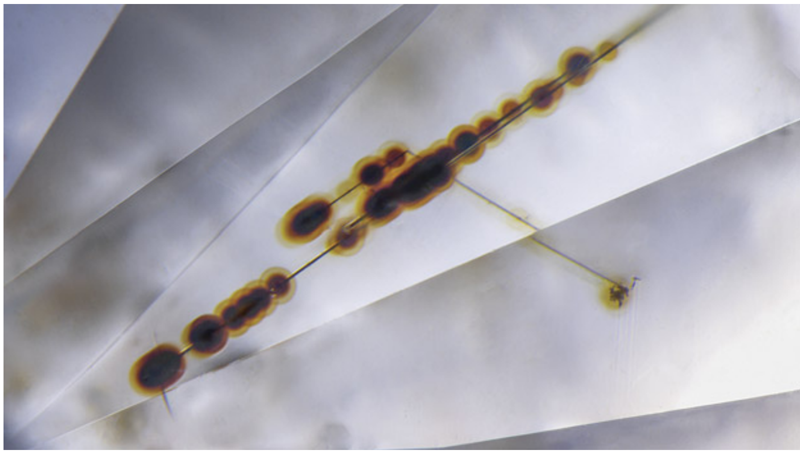

Figure 3. Five rough diamonds from this study of various colors and habits, displaying natural radiation staining. These samples originate from Guyana except for the second from the right, which is reportedly from Venezuela. Carat weights from left to right are 0.01 ct (Guy304), 0.04 ct (Guy572), 0.06 ct (Guy712), 0.11 ct (GV001), and 0.23 ct (Mus17586). Photos by Diego Sanchez.

MATERIALS AND METHODS

Sample Descriptions. A representative sample set of 84 diamonds displaying green and/or brown radiation stains was curated at GIA (figure 3 and table 1). This sample suite consisted of 65 natural rough diamonds collected from the field in Guyana by author RB (see Bassoo et al., 2021), 4 rough diamonds reportedly from Venezuela, 1 rough diamond reportedly from Namibia, and 14 diamonds of unknown provenance. Among the samples of unknown provenance, two were faceted stones submitted to GIA that maintained some natural surfaces and whose color was deemed natural. The samples ranged in size from <0.05 to 1.96 ct (table 1).

The sample set is largely represented by stones from Guyana. However, green diamonds are exceptionally rare globally and Guyana represents one of the few locations where green diamonds are prevalent (Breeding et al., 2018). These are sourced from the Roraima Supergroup, in which diamonds of Guyana, Venezuela, and northern Brazil have resided (Draper, 1951; Santos et al., 2003; Reis et al., 2017). While this dataset serves as a representative example of green diamonds residing in ancient sedimentary rocks of the Roraima Supergroup (Bassoo et al., 2021), expanding the dataset to include more localities where naturally irradiated diamonds are prevalent, such as Zimbabwe or the Central African Republic, will augment this study (e.g., Moore et al., 2009; Smit et al., 2018).

Methods. Radiation stains were imaged in both transmitted and reflected light using a Nikon Eclipse LV100 photomicroscope with 20× (field of view 0.72 mm), 50× (field of view 0.288 mm), and/or 100× (field of view 0.144 mm) objectives. Episcopic or reflected light differential interference contrast (DIC) microscopy was used to increase contrast (Renfro, 2015). A z-stage focus stacking technique was used in which images were stacked together at different focal depths, depending on the flatness of the stone. Step sizes for the 20×, 50×, and 100× objectives were typically 2.5, 0.8, and 0.6 μm, respectively. Stains were cataloged based on notable features, and diameters of rounded stains were measured. Faces of the stones were also imaged to measure the pixel area covered by green and/or brown stains. Four diamonds were imaged at Baylor University in Texas using atomic force microscopy (AFM) with a Bruker Dimension Icon AFM in peak force mode to record and analyze fine surface textures coincident with radiation stains. This technique (box A) precisely measures surface features at a resolution of ~0.1 nm in the Z direction, provided the surface is relatively flat (e.g., Ruiz-Agudo et al., 2009; Fedortchouk, 2019). Depth measurements were compared to a mica specimen, which has a flat and uniform surface with a lateral particle size of less than 5 nm (Ostendorf et al., 2008). The resultant dataset is a micrometer-sized topographic map of a diamond surface. This study defines surface textures coincident with radiation stains as a textural indication of the radiation stains' presence when examining the surface of the rough stone under reflected light, or the presence of features such as cracks and/or ruts in the diamond to which stains are clearly conforming.

TABLE 1. Summary characteristics of radiation stains.

Sample no.	Weight (ct)	Locality	Coincident feature group[a,b]	Shape classification[b]	Radiation stain color	Green surface area per face (%)	Brown surface area per face (%)	Comments on coincident features[b]
Guy012	0.04	Guyana	Group 1	Regular isolated	Green	0.1	—	—
Guy022	0.03	Guyana	Group 1	Regular nondiscrete	Green	0.2	—	—
Guy023	0.03	Guyana	Group 1	Regular nondiscrete	Green	21.2	—	—
Guy078	0.03	Guyana	Group 1	Regular isolated and irregular nondiscrete	Green	12.5	—	—
Guy083	0.01	Guyana	Group 1	Regular nondiscrete and irregular nondiscrete	Green	11.0	—	—
Guy149	0.03	Guyana	Group 1	Regular isolated	Green	6.2	—	—
Guy162	0.02	Guyana	Group 1	Regular isolated and regular nondiscrete	Green	14.8	—	—
Guy186	0.01	Guyana	Group 1	Regular isolated	Green	1.8	—	—
Guy196	0.02	Guyana	Group 1	Irregular isolated	Green	5.6	—	—
Guy197	0.04	Guyana	Group 1	Regular nondiscrete and irregular nondiscrete	Green	8.3	—	—
Guy216	0.04	Guyana	Group 1	Regular isolated and regular nondiscrete	Green	2.6	—	—
Guy221	—	Guyana	Group 1	Irregular isolated	Green	3.0	—	—
Guy231	0.12	Guyana	Group 4	Irregular nondiscrete	Green	26.1	—	Acicular to tabular depressions
Guy239	0.05	Guyana	Group 1	Regular isolated	Green	1.3	—	—
Guy241	0.13	Guyana	Group 1	Regular nondiscrete	Green	2.6	—	—
Guy248	0.06	Guyana	Group 4	Regular nondiscrete and irregular nondiscrete	Green	5.1	—	Subhedral to rounded depressions
Guy264	0.04	Guyana	Group 1	Regular isolated and irregular isolated	Green	1.8	—	—
Guy279	0.10	Guyana	Group 1	Irregular isolated	Green	3.6	—	—
Guy285	0.03	Guyana	Group 1	Irregular nondiscrete	Green	20.6	—	—
Guy304	0.01	Guyana	Group 1	Regular nondiscrete and irregular nondiscrete	Green	21.4	—	—
Guy330	0.04	Guyana	Group 2	Irregular isolated	Green	1.0	—	—

[a]Groups are defined as no coincident surface texture (group 1); rut, crack, or inclusion (group 2); smooth expanded surface (group 3); and surface roughness, acicular, tabular, and other (group 4).
[b]Observed from the region photomicrographed.

TABLE 1 (continued). Summary characteristics of radiation stains.

Sample no.	Weight (ct)	Locality	Coincident feature group[a,b]	Shape classification[b]	Radiation stain color	Green surface area per face (%)	Brown surface area per face (%)	Comments on coincident features[b]
Guy386	0.03	Guyana	Group 1	Regular nondiscrete	Green	0.9	—	—
Guy404	0.13	Guyana	Group 1	Regular isolated	Green	1.4	—	—
Guy504	0.02	Guyana	Group 1	Regular isolated	Green	4.0	—	—
Guy517	0.04	Guyana	Group 1	Regular isolated	Green	1.5	—	—
Guy533	—	Guyana	Group 1	Regular isolated	Green	0.8	—	—
Guy536	0.02	Guyana	Group 1	Irregular nondiscrete	Green	3.8	—	—
Guy551	—	Guyana	Group 1	Regular nondiscrete and irregular nondiscrete	Green	5.4	—	—
Guy562	0.02	Guyana	Group 1	Irregular isolated	Green	5.4	—	—
Guy563	—	Guyana	Group 1	Regular isolated	Green	4.1	—	—
Guy571	0.02	Guyana	Group 1	Regular nondiscrete	Green	8.1	—	—
Guy572	0.04	Guyana	Group 4	Irregular nondiscrete	Green	11.0	—	Subhedral to rounded depressions
Guy593	<0.01	Guyana	Group 1	Regular isolated	Green	4.7	—	—
Guy607	0.02	Guyana	Group 4	Irregular nondiscrete	Green	28.1	—	Fine surface roughness
Guy620	0.01	Guyana	Group 1	Irregular isolated	Green	1.9	—	—
Guy632	0.01	Guyana	Group 1	Regular isolated	Green	1.1	—	—
Guy636	0.01	Guyana	Group 1	Regular isolated	Green	13.5	—	—
Guy651	0.03	Guyana	Group 1	Irregular nondiscrete	Green	22.6	—	—
Guy662	—	Guyana	Group 1	Regular isolated and irregular isolated	Green	3.7	—	—
Guy672	0.05	Guyana	Group 1	Regular isolated	Green	0.3	—	—
Guy678	0.02	Guyana	Group 1	Regular isolated	Green	0.3	—	—
Guy709	0.01	Guyana	Group 1	Regular isolated and irregular isolated	Green	0.2	—	—

[a]Groups are defined as no coincident surface texture (group 1); rut, crack, or inclusion (group 2); smooth expanded surface (group 3); and surface roughness, acicular, tabular, and other (group 4).
[b]Observed from the region photomicrographed.

TABLE 1 (continued). Summary characteristics of radiation stains.

Sample no.	Weight (ct)	Locality	Coincident feature group[a,b]	Shape classification[b]	Radiation stain color	Green surface area per face (%)	Brown surface area per face (%)	Comments on coincident features[b]
Guy710	0.01	Guyana	Group 1	Regular nondiscrete and irregular nondiscrete	Green	3.4	—	—
Guy711	—	Guyana	Group 1	Regular isolated	Green	2.0	—	—
Guy712	0.06	Guyana	Group 1	Regular isolated, regular nondiscrete, and irregular nondiscrete	Green	4.4	—	—
Guy713	0.03	Guyana	Group 1	Regular isolated	Green	17.0	—	—
Guy714	0.03	Guyana	Group 1	Regular isolated	Green	0.2	—	—
Guy715	0.01	Guyana	Group 1	Irregular nondiscrete	Green	16.4	—	—
Guy717	0.07	Guyana	Group 1	Regular isolated	Green	0.8	—	—
Mus17586	0.23	Guyana	Group 1	Irregular nondiscrete	Green	8.3	—	—
JK001	0.16	Namibia	Group 3	Regular isolated	Green	0.9	—	—
2845	0.97	Unknown	Group 4	Irregular nondiscrete	Green	—	—	Acicular to tabular depressions
3810	0.06	Unknown	Group 4	Regular nondiscrete and irregular nondiscrete	Green	93.4	—	Fine surface roughness
3825	0.05	Unknown	Group 1	Irregular nondiscrete	Green	11.3	—	—
3842	0.03	Unknown	Group 1	Irregular nondiscrete	Green	25.6	—	—
9018	1.96	Unknown	Group 2	Irregular nondiscrete	Green	—	—	—
GS-7	0.09	Unknown	Group 4	Irregular nondiscrete	Green	31.0	—	Subhedral to rounded depressions
GS-9	0.12	Unknown	Group 4	Regular nondiscrete and irregular nondiscrete	Green	18.0	—	Fine surface roughness
Mus12308	0.10	Unknown	Group 4	Regular isolated and irregular nondiscrete	Green	21.2	—	Fine surface roughness
Mus24646	0.02	Unknown	Group 1	Irregular nondiscrete	Green	31.1	—	—
Mus31608	0.17	Unknown	Group 4	Regular nondiscrete and irregular nondiscrete	Green	1.2	—	Subhedral to rounded depressions
RH001	0.04	Unknown	Group 4	Regular nondiscrete	Green	19.1	—	Subhedral to rounded depressions
RH002	0.05	Unknown	Group 4	Irregular nondiscrete	Green	23.7	—	Subhedral to rounded depressions

[a]Groups are defined as no coincident surface texture (group 1); rut, crack, or inclusion (group 2); smooth expanded surface (group 3); and surface roughness, acicular, tabular, and other (group 4).
[b]Observed from the region photomicrographed.

TABLE 1 (continued). Summary characteristics of radiation stains.

Sample no.	Weight (ct)	Locality	Coincident feature group[a,b]	Shape classification[b]	Radiation stain color	Green surface area per face (%)	Brown surface area per face (%)	Comments on coincident features[b]
SM001	0.03	Unknown	Group 1	Irregular nondiscrete	Green	28.6	—	—
GV001	0.11	Venezuela (Guaniamo area)	Group 4	Irregular nondiscrete	Green	35.1	—	Acicular to tabular depressions
GV002	0.06	Venezuela (Guaniamo area)	Group 4	Regular isolated and irregular nondiscrete	Green	15.1	—	Fine surface roughness
GV003	0.05	Venezuela (Guaniamo area)	Group 4	Irregular isolated	Green	8.3	—	Acicular to tabular depressions
GV004	0.02	Venezuela (Guaniamo area)	Group 4	Regular isolated and irregular isolated	Green	10.5	—	Etched surface
Guy515	0.03	Guyana	Group 4	Irregular nondiscrete	Brown	—	7.9	Surface roughness
Guy529	0.02	Guyana	Group 1	Irregular nondiscrete	Brown	—	12.1	—
Guy553	0.04	Guyana	Group 1	Regular isolated	Brown	—	1.5	—
Guy046	0.02	Guyana	Group 1	Regular nondiscrete	Green and brown	4.3	<0.1	—
Guy099	0.03	Guyana	Group 1	Irregular isolated	Green and brown	1.9	0.2	—
Guy120	0.02	Guyana	Group 1	Regular nondiscrete	Green and brown	0.8	<0.1	—
Guy126	0.03	Guyana	Group 1	Regular nondiscrete	Green and brown	1.0	0.3	—
Guy156	0.05	Guyana	Group 4	Regular isolated and irregular isolated	Green and brown	2.9	<0.1	Fine surface roughness
Guy501	0.01	Guyana	Group 1	Regular isolated	Green and brown	1.0	<0.1	—
Guy503	0.01	Guyana	Group 1	Regular nondiscrete	Green and brown	0.5	0.5	—
Guy516	0.02	Guyana	Group 1	Regular isolated	Green and brown	0.5	0.3	—
Guy622	0.03	Guyana	Group 4	Regular isolated, regular nondiscrete, and irregular nondiscrete	Green and brown	7.2	1.5	Acicular to tabular and subhedral to rounded depressions
Guy631	0.03	Guyana	Group 1	Regular isolated	Green and brown	0.4	3.7	—
Guy708	0.05	Guyana	Group 1	Irregular nondiscrete	Green and brown	7.0	6.4	—
Guy716	0.02	Guyana	Group 1	Regular nondiscrete and irregular nondiscrete	Green and brown	7.9	0.2	—
7682	1.86	Unknown	Group 4	Regular isolated and regular nondiscrete	Green and brown	42.4	<0.1	Subhedral to rounded depressions

[a]Groups are defined as no coincident surface texture (group 1); rut, crack, or inclusion (group 2); smooth expanded surface (group 3); and surface roughness, acicular, tabular, and other (group 4).
[b]Observed from the region photomicrographed.

BOX A: ATOMIC FORCE MICROSCOPY

Atomic force microscopy (AFM) is a micro-imaging technique that uses a sharp tip to move across a surface, recording the topography and elevation differences in the Z direction as it scans across the surface in the X and Y directions. The tip is typically made of silicon or silicon nitride and is reusable due to its relative hardness. The tip is attached to an optical lever or cantilever, which is in the optical path of a laser and photodetector. When the cantilever moves across the surface, it bends up and down, and a laser reflects from the back of the cantilever onto a photodetector with each motion of the cantilever (figure A-1). The angular motion of the cantilever causes the recorded position of the laser to change accordingly. In "peak force tapping mode" devices, the cantilever oscillates within 0.1–10 nm of the sample surface and never makes contact. Instead, forces repel the tip when in close proximity to the surface. These configurations significantly reduce tip and sample surface damage. A piezoelectric scanner measures and monitors the X, Y, and Z directions as the cantilever moves according to instrument-appropriate and preselected maximums to prevent any damage from occurring. The position data is recorded across the surface of a material. The signals are turned into a 3D image of the surface (e.g., Eaton and West, 2010; figure A-2). Cross-sectional profiles of topography across different regions of the 3D maps can be drawn (figure A-2) and numerical data for heights and depths recorded.

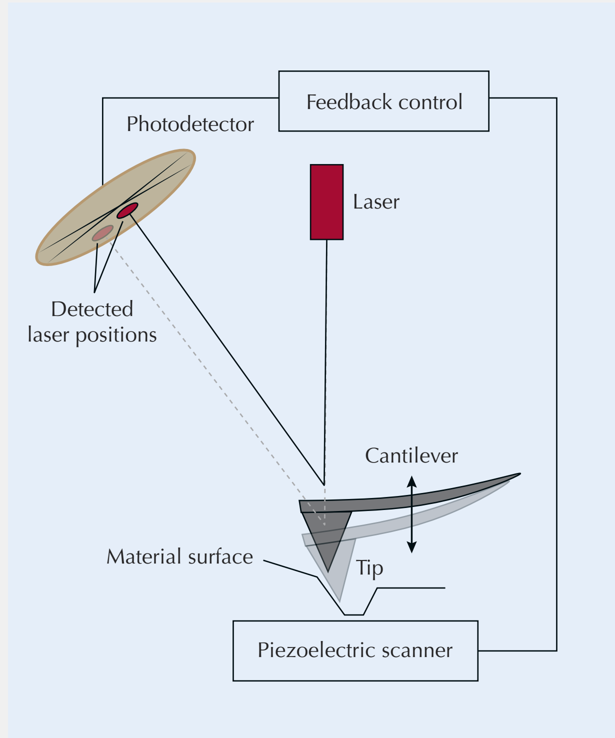

Figure A-1. Schematic demonstrating the basic principle of atomic force microscopy.

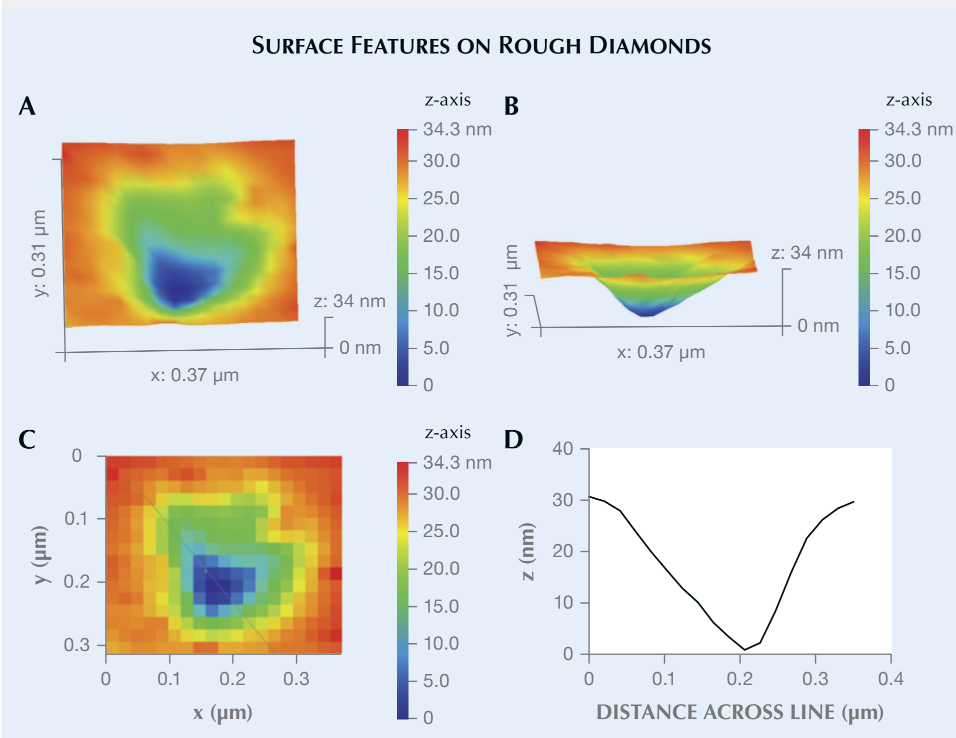

Figure A-2. Surface features on rough diamonds can be documented through AFM and viewed at various angles in 3D (A and B). Lines can be drawn at any point on a 2D heat map (C) and a cross-sectional profile (D) extracted. This triangular-shaped pit has features consistent with a trigon.

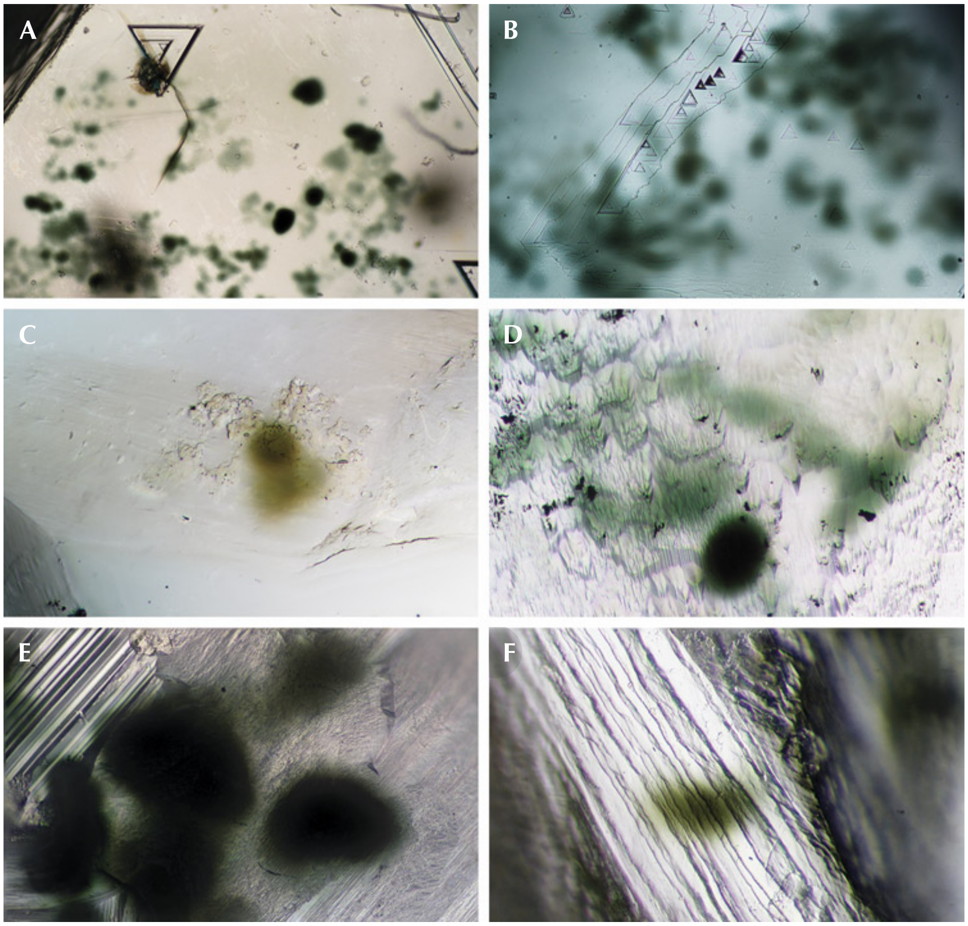

Figure 4. Radiation stains on surfaces of rough diamonds from Guyana, displaying variability in shape, hue, size, and opacity. Photomicrographs by Taryn Linzmeyer; fields of view 1.44 mm (A), 0.72 mm (B), and 0.288 mm (C–F).

RESULTS

Radiation stains in the samples varied in color, morphology, and texture (figure 4), with some inter-stain variability within the same stone. Variations in opacity, color, dominant shape, and coincident surface textures found in natural radiation stains on diamonds were documented as observed through photomicrography. Preliminary AFM measurements of negative surface textures coincident with radiation stains are also presented. These features have rarely been documented (Mendelssohn, 1971; Eaton-Magaña and Moe, 2016; Bassoo, 2022) and to our knowledge have never been documented by AFM in published literature.

Color and Opacity. Most of the diamonds contained only green radiation stains, accounting for 81% of the samples in this study. Solely brown radiation stains were observed on about 3.5% of the diamonds, and brown and green radiation stains occurred together in 15.5% of the samples. Green radiation stains covered <1–93% of a diamond's total surface area, with most in the range of <1–25%. Brown radiation stains in this study covered <1% to up to 12% of a diamond's surface area. Diamonds from other localities such as Zimbabwe often have brown radiation stains over a larger proportion of their surface area (Smit et al., 2018). Opacity ranges from opaque to translucent.

Shape and Size. About 42% of the diamonds displayed radiation stains that were exclusively circular to oval in shape in the field of view. Circular radiation stains ranged in diameter from 22 to 77 μm, with a median of 34 ± 5 μm (figure 5; see appendix 1 at https://www.gia.edu/gems-gemology/spring-2026-radiation-stains). (Uncertainties are reported to one median absolute deviation, or MAD.) Oval radiation stains ranged in long-axis diameter from ~36 to 158 μm with a median of 68 ± 18 μm, whereas the short-axis diameter ranged from 25 to 104 μm, with a median of 42 ± 6 μm (figure 5; see appendix 1). Solely irregularly shaped radiation stains occurred in about 33% of the

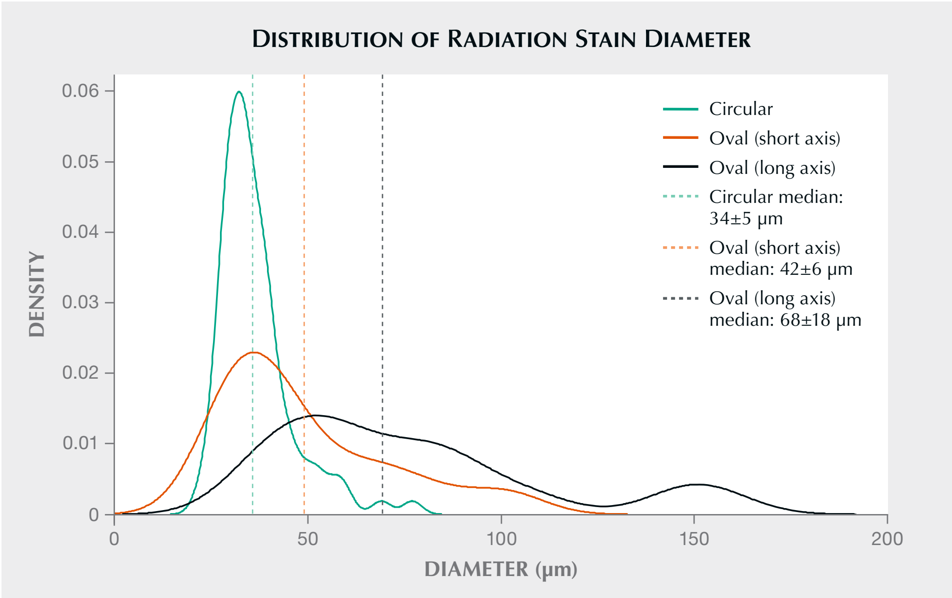

Figure 5. Kernel density estimate (KDE) plot of the diameter of circular radiation stains and the major and minor axes of oval radiation stains. KDE is similar to a histogram, but it is a method of plotting that is independent of arbitrary "bins."

diamonds, whereas about 24% of the samples displayed both regular and irregular radiation stains. Irregularly shaped radiation stains occurred as large lobate or mesh-worked patches of green color, or they corresponded with agglomerations of individual circular or oval radiation stains connected by translucent or diffuse "halos."

Underlying Surface Features Coincident with Radiation Stains. Approximately 73% of the diamonds examined in this study showed no obvious surface textures coincident with the radiation stains imaged. Underlying surface textures coincident with radiation stains included ruts, cracks, expanded rounded surfaces, and fine surface irregularities (figure 6). Diamonds with ruts or cracks corresponding with radiation stains accounted for 2% of the samples. The sole diamond from Namibia had smooth positive relief coincident with the radiation stain (figure 6, E and F). In samples Guy572 and Guy515, surface roughness corresponded with the most opaque regions of the radiation stains and did not extend all the way

Figure 6. Underlying surface textures coincident with radiation stains. Samples RH001 (A and B), GV003 (C and D), JK001 (E and F), and Guy330 (G and H) are shown. A–D display etching coincident with radiation stains. Surface textures in B and D are noted by arrows. E and F show positive relief at the site of a radiation stain on a Namibian diamond. G and H show radiation stains coincident with ruts at the surface of the diamond. These are imaged in transmitted light (A, C, E, and G) along with the corresponding false-color DIC images (B, D, F, and H). Image B's brightness and contrast were adjusted to increase visibility of the topography. Photomicrographs by Taryn Linzmeyer; fields of view 0.144 mm (A and B), 0.451 mm (C and D), and 0.288 mm (E–H).

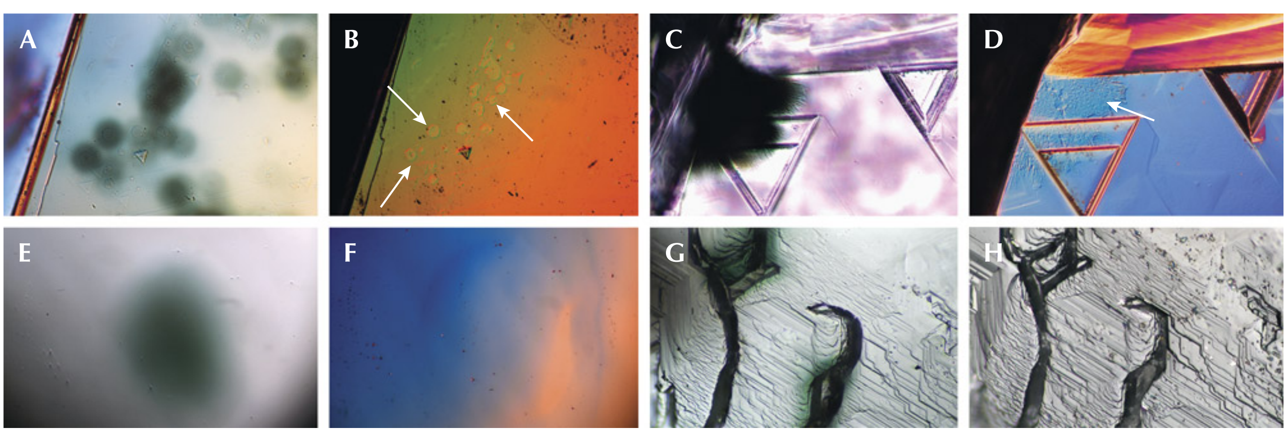

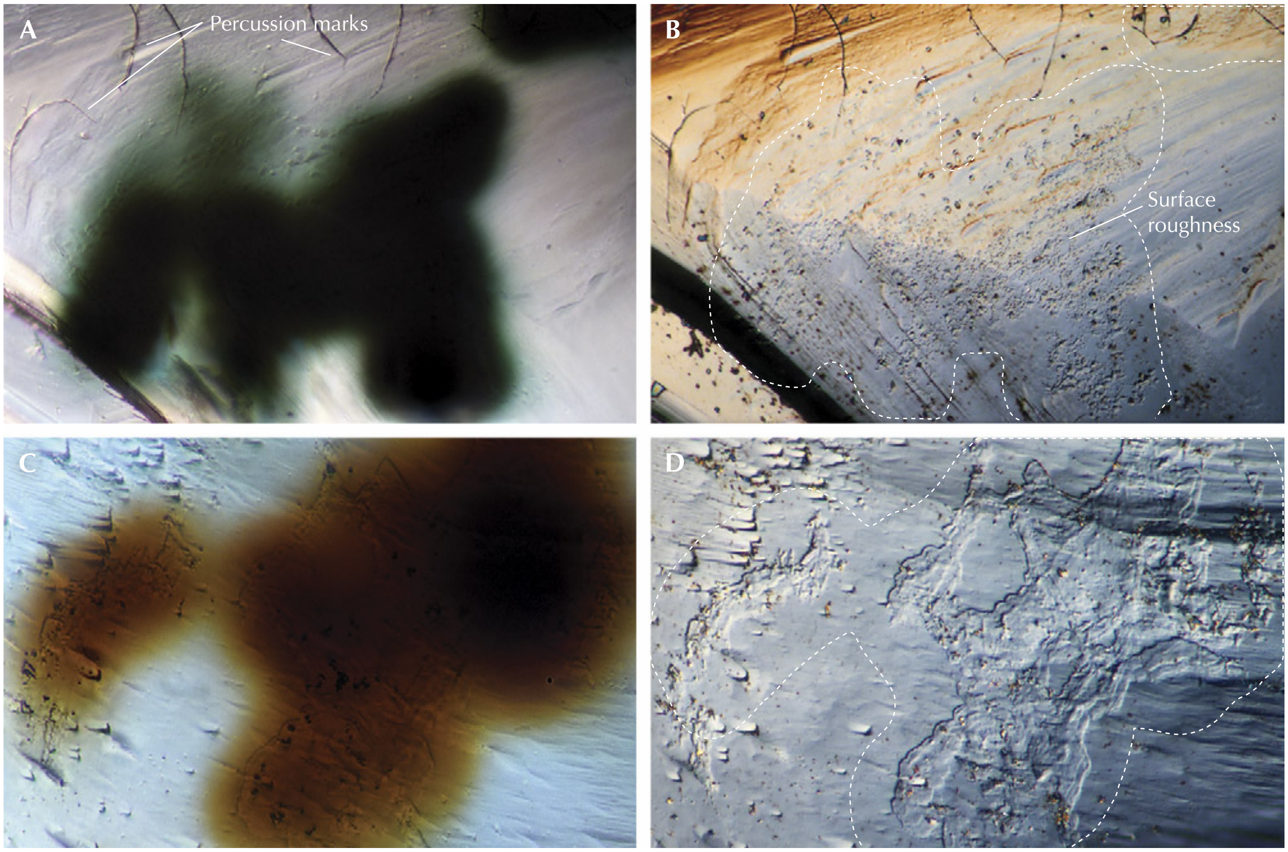

Figure 7. Samples Guy572 (A and B, field of view 0.288 mm) and Guy515 (C and D, field of view 0.144 mm) display surface textures coincident with green (A) and brown (C) radiation staining. The surface roughness in B contains rounded pits. Percussion marks labeled in A are abrasion and transport features typically associated with placer diamonds such as these. Reflected light images were taken using white-balanced DIC settings to increase shadow contrast. Photomicrographs by Taryn Linzmeyer.

to the margins (figure 7). For example, Guy515's surface roughness extended to a maximum distance of ~18 μm from the diffuse margin of the radiation stain edge. In all, 24% of the diamonds had either fine irregular surface roughness coincident with radiation stains or fine acicular (figure 8, opposite page), tabular, or rounded (figure 9) surface textures coincident with radiation stains. Preliminary AFM measurements verified that these were negative surface features penetrating into the surface of the diamond.

DISCUSSION

Color. The radiation stains in this study were green or brown. Pink radiation stains do occur, but they are extremely rare and to our knowledge have only been reported in two diamonds (Breeding et al., 2022).

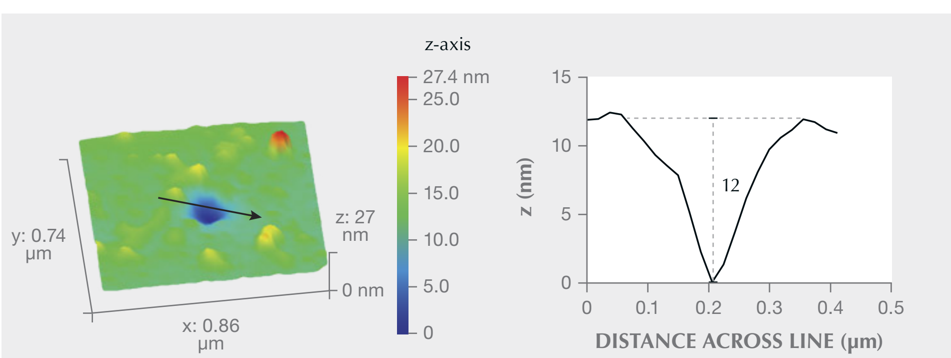

Figure 9. AFM data of etch pits collected on a radiation stain on Guy622. The location and direction in which the cross-sectional profile was drawn is labeled by a black arrow on the left.

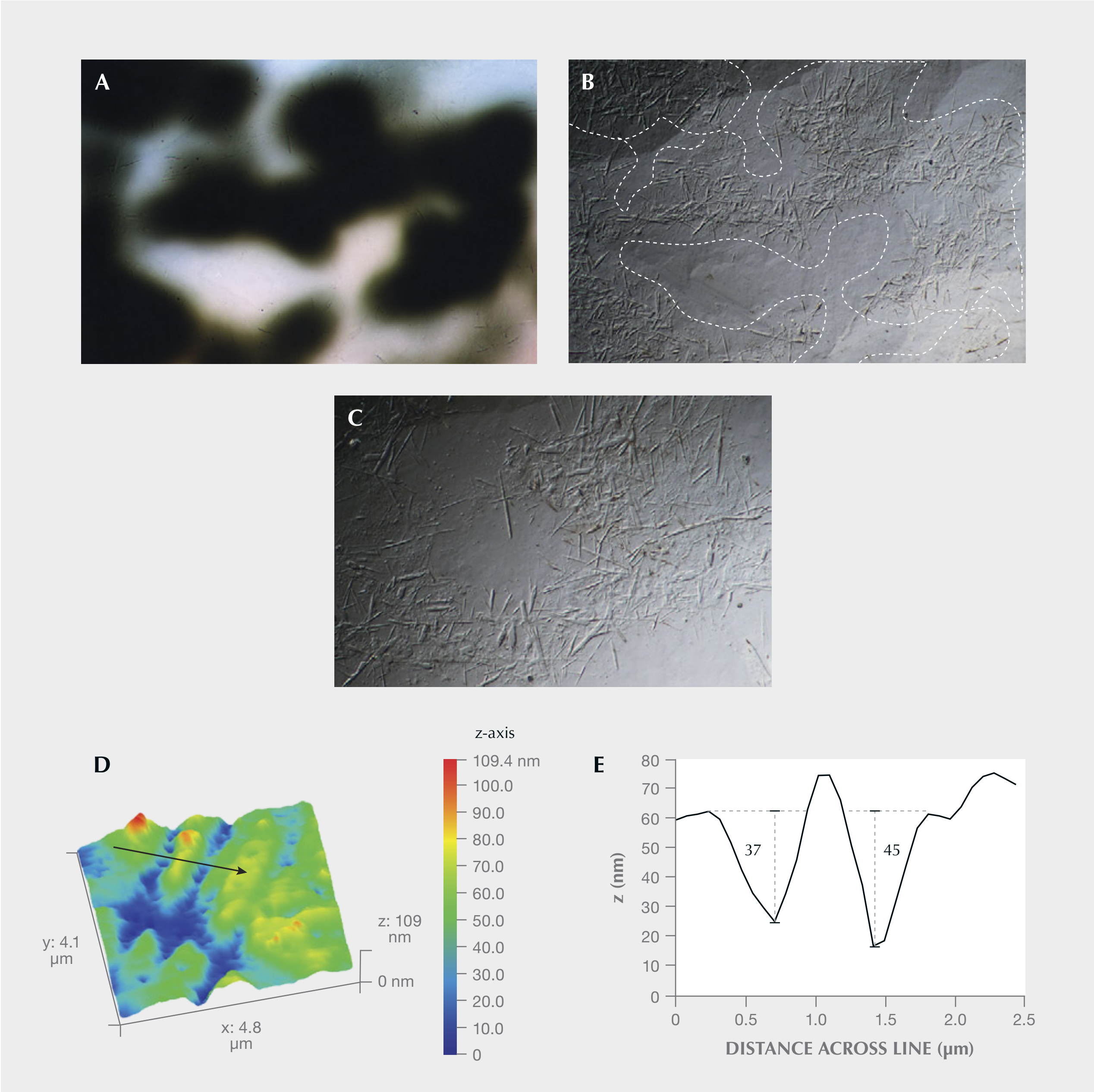

Figure 8. Sample Guy231, photographed in transmitted light (A) and white-balanced DIC (B), displays acicular etching coincident with radiation staining; field of view 0.288 mm. The DIC region using 100× magnification is shown in C; field of view 0.144 mm. Photomicrographs by Taryn Linzmeyer. AFM data was also collected on this sample, displaying the depth of some acicular etches coincident with the stain as a 3D diagram (D) and as a cross-sectional profile (E). The location and direction of the cross-sectional profile is labeled by a black arrow in D.

Radiation stains may vary in opacity between stains on the same diamond or even within the same stain. Variations in opacity within the same stain can occur in the form of radiation "halos," which may appear as translucent rims surrounding more opaque cores. The separation between opaque cores and translucent rims can be diffuse or have sharp boundaries (again, see figure 2). The exact mechanism causing this variation in opacity is unknown, and the following theories are speculative.

In large areas of opaque radiation staining, this may indicate a radioactive grain in direct contact with the surface of the diamond, with alpha radiation penetrating farther as a halo. Variable opacities and

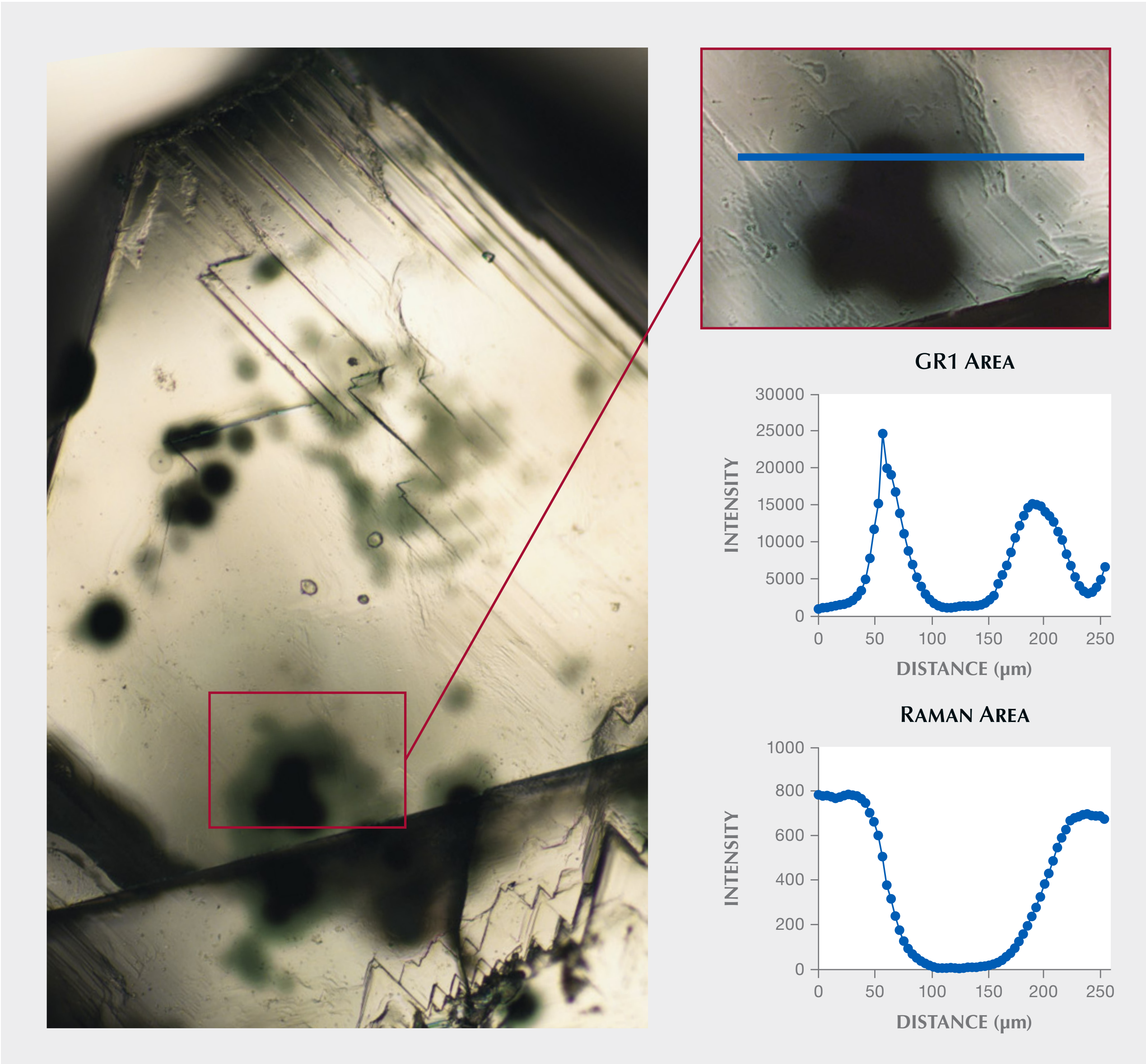

Figure 10. Left: Radiation stains displaying both opaque and translucent staining are shown in Guy651. Photomicrograph by Taryn Linzmeyer; field of view 0.70 mm. Right: Using 633 nm laser excitation, PL spectra were collected at liquid nitrogen temperature along a line transecting "clean" diamond surfaces, translucent radiation staining, and opaque radiation staining (blue line, top right). The pixel size for each spectrum was 3.8 µm. The map was split into a horizontal transect. There are 204 spectra plotted in each of these graphs, with three spectra averaged for each point in the y direction. The intensity of the GR1 is highest in regions of translucent staining and falls off in the opaque regions, despite these regions being intensely irradiated. This is consistent with the intense damage to the diamond structure resulting in a weaker Raman response, as shown in the decrease of the diamond Raman peak at 691 nm.

saturations of green color may be related to variable exposure time and/or concentrations of radioactive minerals (Nasdala et al., 2013; Vasilev et al., 2018). For example, evidence of greater damage to the diamond structure in areas of opaque staining was observed using photoluminescence (PL) mapping of an opaque stain with a translucent halo (figure 10). GR1 peak areas increased in translucent radiation staining compared to a "clean" diamond surface but decreased significantly in the area of opaque staining.

BOX B: RADIATION DAMAGE EXTENDING BELOW THE SURFACE OF A DIAMOND

Damage to the diamond structure due to alpha particle radiation also extends below the surface. Previous studies used the peak area of the diamond Raman band as a proxy for the extent of damage, with decreasing peak areas and a sharpening peak shape into the stone signifying a transition from amorphous carbon to undamaged diamond (Eaton-Magaña and Moe, 2016). Distortion of the diamond Raman band (1332 cm^{-1}) and other peaks is observed within radiation stains (figure B-1). This supports the premise that alpha radiation may damage the diamond structure to ~25–30 μm below the surface following irradiation (Eaton-Magaña and Moe, 2016).

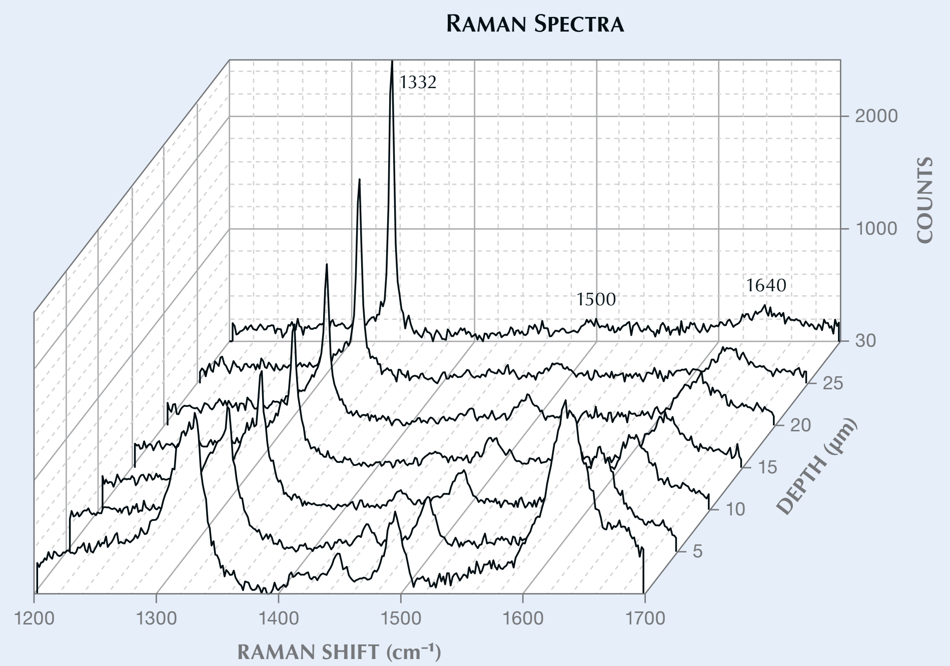

Figure B-1. Raman spectra as a function of depth into a diamond from the surface. This shows how the diamond Raman band at 1332 cm^{-1} (with 514 nm excitation) changes with depth starting at the surface of a heavily irradiated stain. At the surface, the diamond Raman band becomes broader and includes extra peaks consistent with altered carbon states. Adapted from Eaton-Magaña and Moe (2016).

This is due to the extreme damage to the diamond structure, as evidenced by the much lower Raman signal (box B).

Another factor that may affect the opacity of the stain is the separation distance through which the alpha particle travels. For example, a greater separation distance would permit fewer alpha particles to reach a diamond's surface and create the vacancies leading to green color.

In some cases, both green and brown radiation stains are found adjacent to each other on the same diamond (figure 11). The transition from green to brown radiation stains indicates exposure to annealing temperatures of 550–600°C for short periods or, more likely, at lower annealing temperatures over geologic timescales (Vance et al., 1973; Koivula, 2000; Eaton-Magaña and Moe, 2016; Breeding et al., 2018; Eaton-Magaña et al., 2023). These stains of different colors sometimes connect, indicating shifting of the diamond relative to the radioactive source and subsequent re-irradiation (e.g., Schulze and Nasdala, 2016).

Shape. Radiation stains on diamond surfaces can occur on all faces, which suggests that diamonds can be irradiated from external point sources from various directions (Schulze and Nasdala, 2016). When alpha particles bombard a diamond surface, they dislodge a collection of carbon atoms that cascade outward and away from the initial point of impact to simultaneously create vacancies and interstitials (Raal and Robinson, 1980; Koptil and Zinchuk, 2000; Breeding et al., 2018). In this study, many instances of circular radiation stains were observed. The diameter of this circle may be related to the maximum

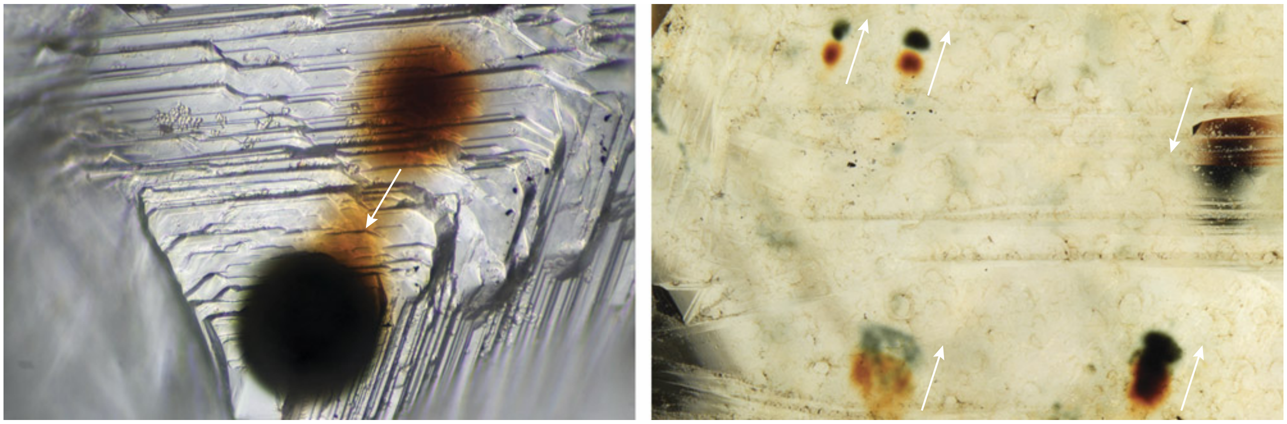

Figure 11. Photomicrographs of radiation stains demonstrating shifting. Left: Green and brown radiation staining on a rough diamond from Guyana (Guy503). The similar size and shape of the round radiation stains, as well as the diffuse staining connecting the two more opaque centers, indicates that this diamond either experienced heating and subsequent cooling before the deposition of the newer green radiation stain or was subjected to different irradiation events over time (e.g., Vance et al., 1973; Raal and Robinson, 1980). The direction that the irradiated region changed over time is indicated by an arrow, from older to newer staining. Photomicrograph by Taryn Linzmeyer; field of view 0.288 mm. Right: Multiple stages of shifting are indicated by the two directions of displacement of the older brown and younger green stains (upward-pointing arrows indicate stains on the top surface of the diamond, and the downward-pointing arrow indicates a view through the diamond to radiation stains located on the bottom surface). Photomicrograph by Sally Eaton-Magaña; field of view 3 mm. Modified from Ardon and Eaton-Magaña (2020).

lateral dispersal of vacancies and interstitials created during alpha particle irradiation. From the surface plane, the circular radiation stains documented in the samples ranged in diameter from 22 to 77 μm.

Oval- and elongate-shaped radiation stains may indicate alpha radiation coinciding with either slight movement of the diamond relative to the radioactive mineral or a radioactive mineral with a non-spherical shape, causing the area of irradiation to present as slightly elongate. These shapes may also arise from multiple circular stains overlapping to create an oval shape. For those diamonds with radiation stains over much of their surface area, this is likely caused by multiple radiation events and/or radiation sources that occurred during erosion and continuous redeposition within the paleoplacer environment (e.g., Koivula, 2000; Chaves et al., 2001; Santos et al., 2003). Interconnected brown and green radiation stains and irregular agglomerations of radiation stains provide evidence of multiple irradiation events over time (figure 11).

The cause of radiation stain shapes is complex and likely influenced by factors such as diamond surface topography, radioactive mineral habit, relative orientation and separation of diamond to the radiation source, and radiation type. Notwithstanding that, radiation stain morphologies are classifiable and certainly warrant further study.

Surface Features Coincident with Radiation Stains. Rough diamonds display surface textural features that reflect their journey from residence in the mantle, eruption to the earth's surface, and for some, subsequent alluvial transport. Etching can modify diamond surfaces, typically beginning at sites of geometric imperfections such as dislocations (Wilks and Wilks, 1994; Smit and Shirey, 2020). Dissolution features may develop in the mantle and/or kimberlite or lamproite melt, several of which are dependent on diamond morphology. These features are not related to radiation stains, and in most cases they are not coincident. For example, trigons, hexagons, and shield-shaped laminae are found on octahedral faces. However, tetragons are found on cubic faces, while hillocks and terraces are found on dodecahedral faces (Tappert and Tappert, 2011; Harris et al., 2022) (figure 12). Late-stage etching in kimberlite can result in textures such as corrosion sculptures, shallow depressions, and circular micro-disks and micro-pits. Most diamonds in this study had a placer origin and thus had surface textures consistent with late-stage abrasion and transport, such as network patterns or crescent-shaped percussion marks (Tappert and Tappert, 2011; Harris et al., 2022).

Fine negative surface topographies coincident with radiation stains were observed resulting from uncommon irradiation and dissolution conditions.

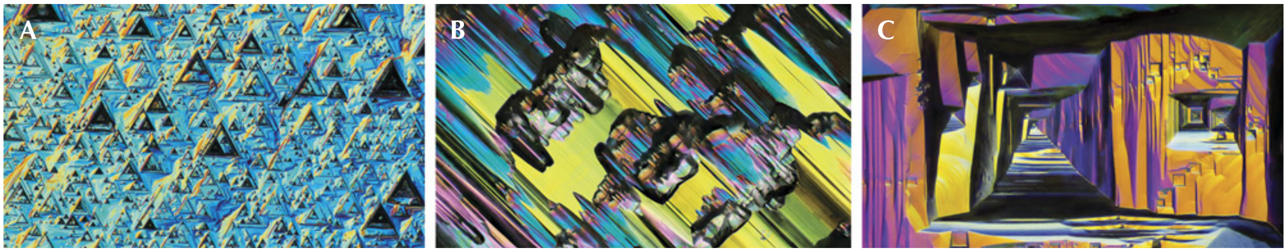

Figure 12. False-color DIC images of typical surface textural features in rough diamond. These include trigons (A), hillocks (B), and tetragons (C). Photomicrographs by Nathan Renfro; fields of view 0.72 mm (A), 1.44 mm (B), and 2.88 mm (C).

In some cases, microscopic raised surface features tended to partially infill obvious rounded pits. The composition of these infill features have not been identified, but some may be surface contamination such as dust particles (Nasdala et al., 2013).

Ruts were also observed, which are formed by diamond dissolution along fractures or cracks, causing them to widen (Tappert and Tappert, 2011; Harris et al., 2022). Subsequently, radioactive minerals can precipitate from percolating fluids (Finch and Murakami, 1999; Hazen et al., 2009; Lauf, 2016) into ruts or cracks when diamonds reside in alluvial environments. This can result in green coloration coincident with these surface dissolution features. Stains can also reflect grain boundaries between adjacent minerals or grains, leaving radiation stains in a meshwork pattern (figure 13; Nasdala et al., 2013; Breeding et al., 2018).

The updoming seen in some diamonds (figure 13) likely reflects volumetric surface expansion during irradiation (e.g., Meyer et al., 1965; Vance and Milledge, 1972; Dooley et al., 1993; Bosia et al., 2011; Nasdala et al., 2013). Additionally, in 6% of the samples, we observed fine acicular to tabular depressions from etching (again, see figure 8) that closely mirrored the outline of radiation stains. These features are not observed outside of radiation stains and cross-cut mantle dissolution textures (Bassoo, 2022; Stephan et al., 2022). Dissolution features such as trigons can penetrate significantly deeper into the diamond, in some cases hundreds to thousands of nanometers deep (Fedortchouk et al., 2011; Fedortchouk, 2019).

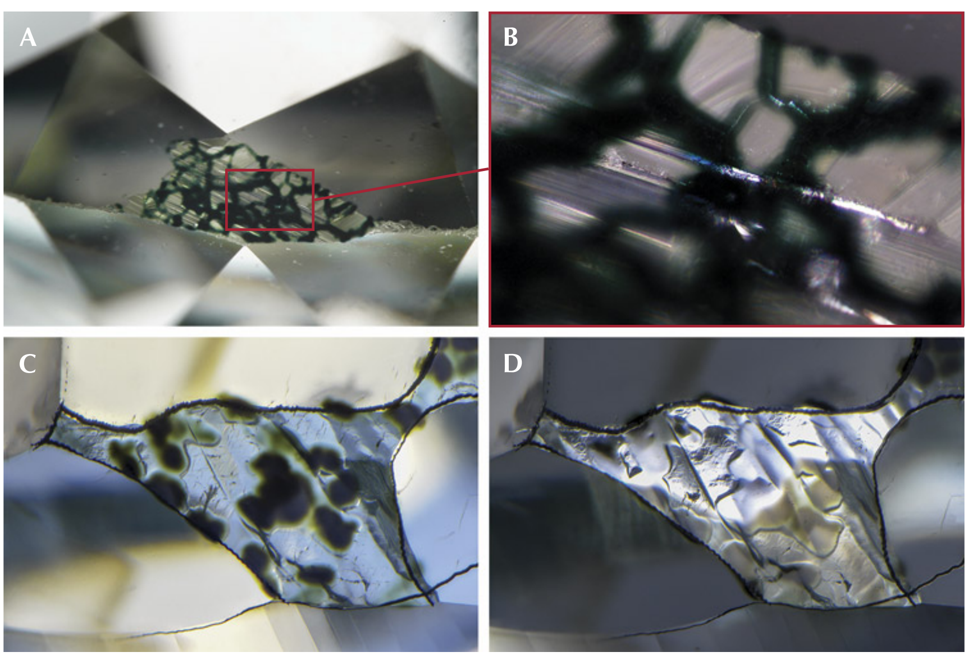

Figure 13. Faceted diamonds with preserved natural surfaces. A and B: Radiation staining coincident with cracks in the surface. This staining is likely deposited by radioactive fluids seeping through the cracks of adjacent mineral grains, resulting in a meshwork pattern. Photomicrographs by Taryn Linzmeyer; fields of view 3.57 mm and 0.72 mm. C and D: Radiation staining coincident with smooth, expanded surfaces. Image D was taken in reflected light to emphasize the surface topography. Photomicrographs by Nathan Renfro; field of view 2.24 mm. From Ardon (2021).

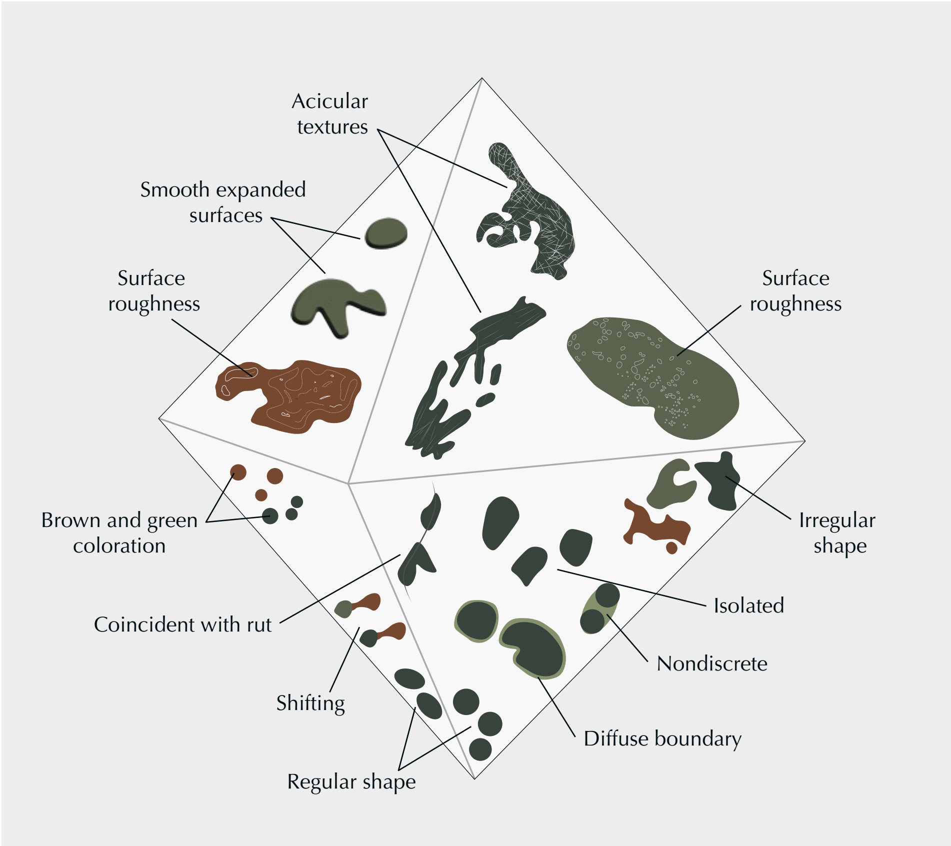

Figure 14. A schematic representation of radiation stain features.

AFM measurements confirmed that both acicular and rounded pits were relatively shallow (figures 8 and 9) and had a smooth topography consistent with diamond dissolution. Previous studies have shown that irradiated diamond surfaces are more prone to etching at the site of irradiation (Mendelssohn, 1971; Mendelssohn et al., 1979). It is likely that highly irradiated sites on a diamond may transition to amorphous carbon such as tetrahedral amorphous carbon (Prawer et al., 1998). Damage to the diamond structure is documented in the broadening and/or weakening of the Raman line in radiation stains (again, see figure 10 and box B; Nasdala et al., 2013; Eaton-Magaña and Moe, 2016; Schulze and Nasdala, 2016) or extra peaks associated with altered carbon states. In the case of acicular-shaped pits, the growth of secondary uranium-bearing minerals with acicular crystal habits may lead to etching. In this scenario, radioactive mineral grains would undergo alteration, leading to the localized formation of smaller secondary crystals with thin acicular habits (e.g., Burns and Hughes, 2003). Subsequently the tetrahedral amorphous carbon would preferentially etch, leaving behind a pit. These etch pits could mirror the morphology of radioactive minerals in physical contact. Future studies of these enigmatic surface features will contribute to our understanding of diamond dissolution in the near-surface environment.

Radiation stain morphology, color, and coincident surface features across a broad range of diamonds (figure 14) permit the development of a new radiation stain classification scheme (figure 15). The classification may be used to describe individual radiation stains or regions of staining.

Color. This study identifies green and brown as near-exclusive colors of diamond radiation stains. The green color can be very dark green, appearing almost black.

Opacity. The radiation stains varied widely in opacity from opaque to nearly transparent. These may be classified as opaque or translucent. This classification could help to distinguish the degree of structural damage experienced by a diamond population due to irradiation. In most cases, natural radiation stains with an opaque center occur within translucent boundaries. In nondiscrete staining with multiple opaque centers, translucent staining connecting the dominant shapes is implied (see next section).

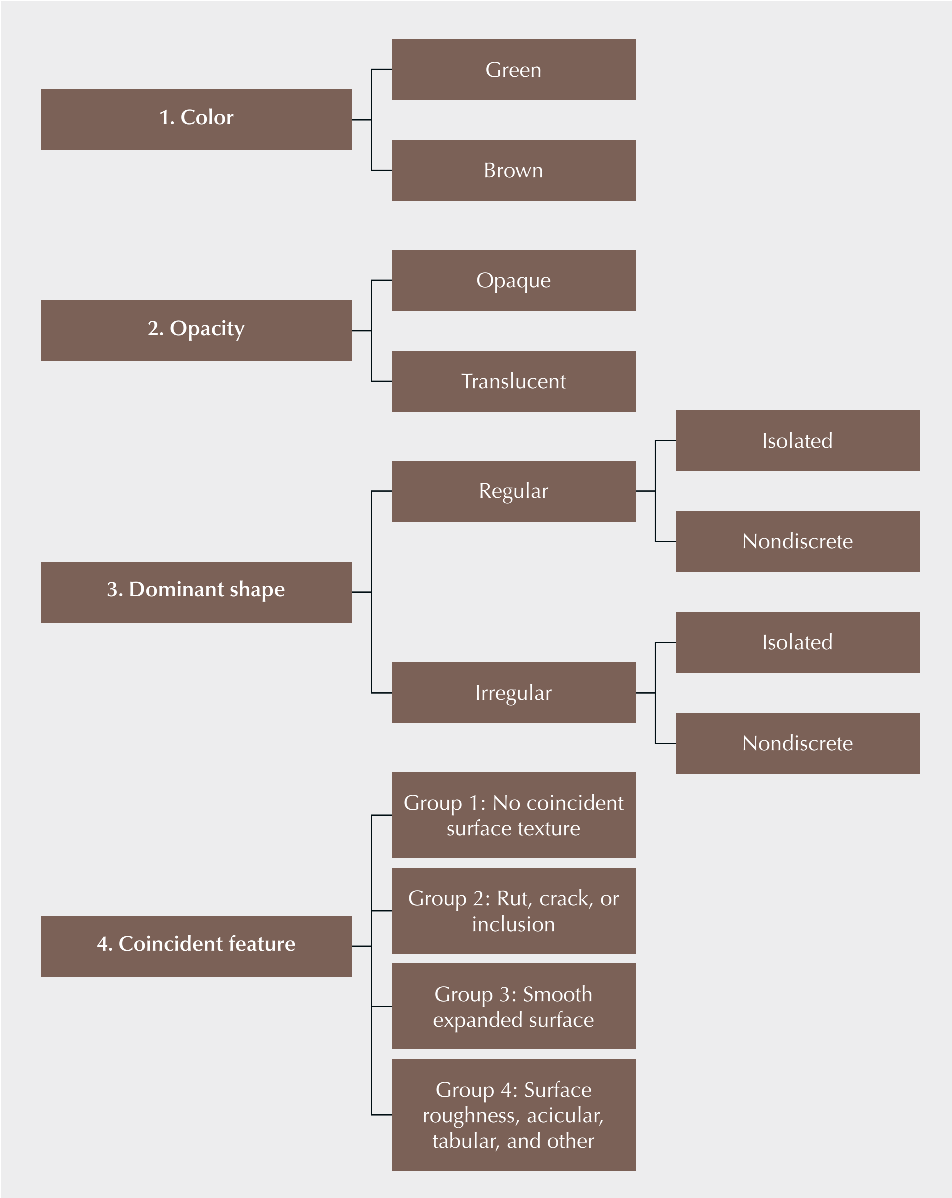

Figure 15. A proposed classification scheme for radiation stains on diamond.

Dominant Shape. The shapes of radiation stains can be classified by their dominant shape as either regular or irregular. This is the most opaque region of the stain. The terms *regular* can be used to encompass stains of both circular and oval shapes and *irregular* to describe all other shapes. To account for stains conjoined with others when their dominant shapes are still visible, regular and irregular radiation stains are subdivided as either "isolated" or "nondiscrete." Stains that are not obviously isolated may be considered nondiscrete. Examples of nondiscrete stains include those with multiple dark, opaque centers connected to one another by diffuse edges or halos in which a clear boundary is ambiguous (figure 16) or stains that are likely associated with radioactive fluids such as those with meshwork patterns. If the dominant shapes are rounded and regular, if not isolated, the stains may be defined as regular nondiscrete (e.g., figure 16H). Some dominant shapes are irregular; if not isolated, they may be considered irregular nondiscrete (e.g., figure 16C).

Multiple radiation stain shapes may occur in close proximity within the same diamond. While in some cases it is very likely that nondiscrete stain types are combinations of what were once rounded and regular point sources, we classify the shapes this way in order to provide terminology devoid of interpretation.

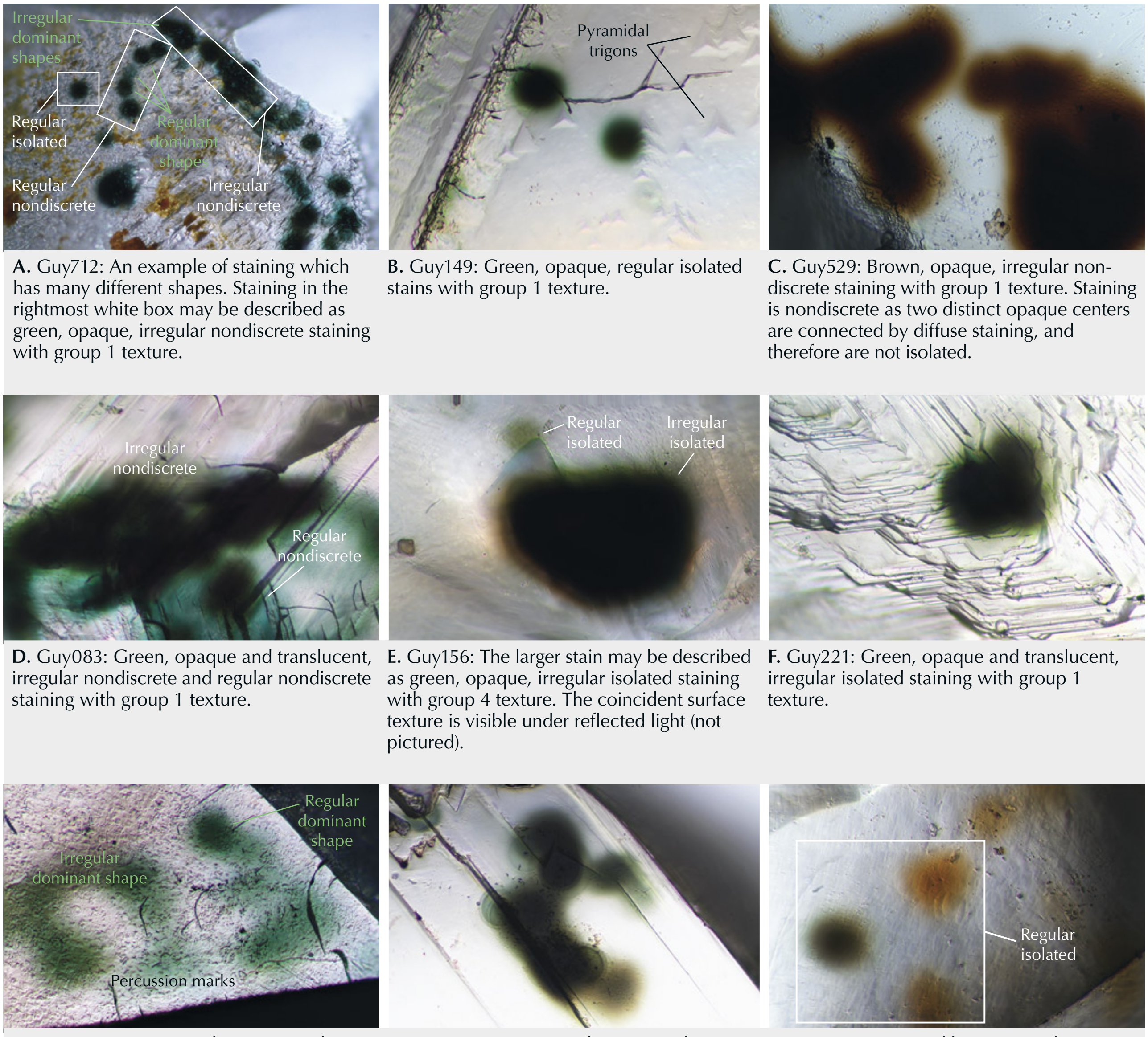

A. Guy712: An example of staining which has many different shapes. Staining in the rightmost white box may be described as green, opaque, irregular nondiscrete staining with group 1 texture.

B. Guy149: Green, opaque, regular isolated stains with group 1 texture.

C. Guy529: Brown, opaque, irregular nondiscrete staining with group 1 texture. Staining is nondiscrete as two distinct opaque centers are connected by diffuse staining, and therefore are not isolated.

D. Guy083: Green, opaque and translucent, irregular nondiscrete and regular nondiscrete staining with group 1 texture.

E. Guy156: The larger stain may be described as green, opaque, irregular isolated staining with group 4 texture. The coincident surface texture is visible under reflected light (not pictured).

F. Guy221: Green, opaque and translucent, irregular isolated staining with group 1 texture.

G. Guy197: Green, translucent, irregular nondiscrete and regular nondiscrete staining with group 1 texture.

H. Guy571: Green, translucent, regular nondiscrete staining with group 1 texture.

I. Guy631: Green and brown, translucent, regular isolated staining with group 1 texture.

Figure 16. Examples of classified radiation stains. Photomicrographs by Taryn Linzmeyer; fields of view 0.72 mm (A) and 0.288 mm (B–I).

Coincident Texture. Several surface textures located coincident with radiation stains were identified and broadly classified into four groups:

- Group 1: No coincident surface texture
- Group 2: Coincident with a rut, etch channel, crack, or inclusion
- Group 3: Smooth expanded surface
- Group 4: Surface roughness, acicular, tabular, and other

CONCLUSIONS

Radiation stains are opaque or translucent, green to brown, and can encompass nearly the entire surface of a diamond. They are regular to irregular in shape and form single isolated or connected zones of nondiscrete patches of color. Circular and oval radiation stains range in diameter from 22 to 158 μm. In this study, almost 25% of the naturally irradiated diamonds had fine surface irregularity coincident with radiation stains, which we term Group 4 textures.

These features can be circular, irregular, or occasionally exhibit fine-scale geometrical characteristics such as fine acicular or tabular negative surface topographies. These textural features coincident with radiation stains may involve localized diamond dissolution in the near-surface environment and warrant future investigation. This study also found that radiation stains have complex but classifiable color, morphological, and textural characteristics.

This classification scheme is intended to provide a framework to describe radiation stains, which are important to the study of irradiated diamonds. Using comprehensive terminology to describe radiation stain morphology and texture will support future studies. Additionally, systematic recording of radiation stains provides a coherent and consistent language for describing naturally irradiated diamonds.

ABOUT THE AUTHORS

Taryn Linzmeyer is an analytics research associate, Dr. Roy Bassoo is a former postdoctoral research associate, Dr. Sally Eaton-Magaña and Nathan Renfro are senior managers of identification, and John I. Koivula is analytical microscopist, at GIA in Carlsbad, California. Dr. Bernd Zechmann is director of the Center for Microscopy and Imaging and a research professor at Baylor University in Waco, Texas.

ACKNOWLEDGMENTS

The authors would like to thank Ulrika D'Haenens-Johansson, Evan Smith, Michael Jollands, Simon Lawson, and Matthew Hardman for their useful suggestions and assistance on earlier versions of this manuscript, as well as three anonymous reviewers for their detailed comments.

REFERENCES

Ardon T. (2021) Micro-World: Expanded diamond surface due to radiation staining. *G&G*, Vol. 57, No.1, pp. 66–67.

Ardon T., Eaton-Magaña S. (2020) Lab Notes: Multiple radiation stains suggest interesting geological residency. *G&G*, Vol. 56, No. 2, pp. 283–285.

Bassoo R. (2022) Micro-World: Acicular troughs coincident with green stains on rough diamond surface. *G&G*, Vol. 58, No.1, pp. 64–65.

Bassoo R., Befus K.S., Liang P., Forman S.L., Sharman G. (2021) Deciphering the enigmatic origin of Guyana's diamonds. *American Mineralogist*, Vol. 106, No. 1, pp. 54–68, https://doi.org/10.2138/am-2020-7486

Beyer S.R., Hiatt E.E., Kyser K., Drever G.L., Marlatt J. (2015) Stratigraphy, diagenesis and geological evolution of the Paleoproterozoic Roraima Basin, Guyana: Links to tectonic events on the Amazon Craton and assessment for uranium mineralization potential. *Precambrian Research*, Vol. 267, pp. 227–249, https://doi.org/10.1016/j.precamres.2015.06.017

Bosia F., Argiolas N., Bazzan M., Olivero P., Picollo F., Sordini A., Vannoni M., Vittone E. (2011) Modification of the structure of diamond with MeV ion implantation. *Diamond and Related Materials*, Vol. 20, No. 5-6, pp. 774–778, https://doi.org/10.1016/j.diamond.2011.03.025

Breeding C.M., Eaton-Magaña S., Shigley J.E. (2018) Natural-color green diamonds: A beautiful conundrum. *G&G*, Vol. 54, No. 1, pp. 2–27, https://doi.org/10.5741/GEMS.54.1.2

Breeding C.M., Price J., Schwartz V., Linzmeyer T. (2022) Pink radiation damage in natural gem diamond. *Geological Society of America Abstracts with Programs*, https://doi.org/10.1130/abs/2022AM-382240

Burns P.C., Hughes K. (2003) Studtite, $[(UO_2)(O_2)(H_2O)_2](H_2O)_2$: The first structure of a peroxide mineral. *American Mineralogist*, Vol. 88, No. 7, pp. 1165–1168, https://doi.org/10.2138/am-2003-0725

Chaves M.L.S.C., Karfunkel J., Hoppe A., Hoover D.B. (2001) Diamonds from the Espinhaço Range (Minas Gerais, Brazil) and their redistribution through the geologic record. *Journal of South American Earth Sciences*, Vol. 14, No. 3, pp. 277–289, https://doi.org/10.1016/S0895-9811(01)00024-4

Clark C.D., Ditchburn R.W., Dyer H.B. (1956) The absorption spectra of natural and irradiated diamonds. *Proceedings of the Royal Society of London. Series A. Mathematical and Physical Sciences*, Vol. 234, No. 1198, pp. 363–381, https://doi.org/10.1098/rspa.1956.0040

Collins A.T. (1982) Colour centres in diamond. *Journal of Gemmology*, Vol. 18, No. 1, pp. 37–75.

Dooley S.P., Jamieson D.N., Prawer S. (1993) He^+ and H^+ microbeam damage, swelling and annealing in diamond. *Nuclear Instruments and Methods in Physics Research Section B: Beam Interactions with Materials and Atoms*, Vol. 77, No. 1-4, pp. 484–491, https://doi.org/10.1016/0168-583X(93)95584-R

Draper T. (1951) The diamond mines of Diamantina—Past and present. *G&G*, Vol. 7, No. 2, pp. 49–57.

Eaton P., West P. (2010) *Atomic Force Microscopy*. Oxford University Press, New York.

Eaton-Magaña S.C., Moe K.S. (2016) Temperature effects on radiation stains in natural diamonds. *Diamond and Related Materials*, Vol 64, pp. 130–142, https://doi.org/10.1016/j.diamond.2016.02.009

Eaton-Magaña S., Breeding C.M., Shigley J.E. (2018) Natural-color blue, gray, and violet diamonds: Allure of the deep. *G&G*, Vol. 54, No. 2, pp. 112–131, https://doi.org/10.5741/GEMS.54.2.112

Eaton-Magaña S., Breeding C.M., Bassoo R. (2023) Low-temperature annealing and kinetics of radiation stains in natural diamond. *Diamond and Related Materials*, Vol. 132, article no. 109649, https://doi.org/10.1016/j.diamond.2022.109649

Fedortchouk Y. (2019) A new approach to understanding diamond surface features based on a review of experimental and natural diamond studies. *Earth-Science Reviews*, Vol. 193, pp. 45–65, https://doi.org/10.1016/j.earscirev.2019.02.013

Fedortchouk Y., Manghnani M.H., Hushur A., Shiryaev A., Nestola F. (2011) An atomic force microscopy study of diamond dissolution features: The effect of H_2O and CO_2 in the fluid on diamond morphology. *American Mineralogist*, Vol. 96, No. 11-12, pp. 1768–1775, https://doi.org/10.2138/am.2011.3828

Finch R., Murakami T. (1999) Systematics and paragenesis of uranium minerals. *Reviews in Mineralogy and Geochemistry*,

Vol. 38, No. 1, pp. 91–179, https://doi.org/10.1515/9781501509193-008
Green B.L., Collins A.T., Breeding C.M. (2022) Diamond spectroscopy, defect centers, color, and treatments. *Reviews in Mineralogy and Geochemistry*, Vol. 88, No. 1, pp. 637–688, https://doi.org/10.2138/rmg.2022.88.12
Harris J.W., Smit K.V., Fedortchouk Y., Moore M. (2022) Morphology of monocrystalline diamond and its inclusions. *Reviews in Mineralogy and Geochemistry*, Vol. 88, pp. 119–166, https://doi.org/10.2138/rmg.2022.88.02
Hazen R.M., Ewing R.C., Sverjensky D.A. (2009) Evolution of uranium and thorium minerals. *American Mineralogist*, Vol. 94, No. 10, pp. 1293–1311, https://doi.org/10.2138/am.2009.3208
Koivula J.I. (2000) *The Microworld of Diamonds*. Gemworld International, Inc., Northbrook, Illinois.
Koptil V.I., Zinchuk N.N. (2000) A change in diamond properties induced by natural radioactive irradiation. *Journal of Superhard Materials*, Vol. 22, No. 2, pp. 56–57.
Lauf R.J. (2016) *Mineralogy of Uranium and Thorium*. Schiffer Publishing, Ltd., Atglen, Pennsylvania.
Mendelssohn M.J. (1971) The etching of diamond and of the associated minerals garnet and olivine. PhD thesis, University of London.
Mendelssohn M.J., Milledge H.J., Vance E.R., Nave E., Woods P.A. (1979) Internal radioactive haloes in diamond. *Diamond Research*, Vol. 17, No. 2, pp. 31–36.
Meyer H.O.A., Milledge H.J., Nave E. (1965) Natural irradiation damage in Ivory Coast diamonds. *Nature*, Vol. 206, p. 392, https://doi.org/10.1038/206392a0
Moore A.E., Cotterill F.P.D., Broderick T., Plowes D. (2009) Landscape evolution in Zimbabwe from the Permian to present, with implications for kimberlite prospecting. *South African Journal of Geology*, Vol. 112, No. 1, pp. 65–88, https://doi.org/10.2113/gssajg.112.1.65
Nasdala L., Grambole D., Wildner M., Gigler A.M., Hainschwang T., Zaitsev A.M., Harris J.W., Milledge J., Schulze D.J., Hofmeister W., Balmer W.A. (2013) Radio-colouration of diamond: A spectroscopic study. *Contributions to Mineralogy and Petrology*, Vol. 165, pp. 843–861, https://doi.org/10.1007/s00410-012-0838-1
Ostendorf F., Schmitz C., Hirth S., Kühnle A., Kolodziej J.J., Reichling M. (2008) How flat is an air-cleaved mica surface? *Nanotechnology*, Vol. 19, No. 30, article no. 305705, https://doi.org/10.1088/0957-4484/19/30/305705
Prawer S., Nugent K.W., Jamieson D.N. (1998) The Raman spectrum of amorphous diamond. *Diamond and Related Materials*, Vol. 7, No. 1, pp. 106–110, https://doi.org/10.1016/S0925-9635(97)00194-5
Raal F.A., Robinson D.N. (1980) Green for rarity. *Nuclear Active*, Vol. 11, No. 23, pp. 5–8.
Reis N.J., Nadeau S., Fraga L.M., Betiollo L.M., Faraco M.T.L., Reece J., Lachhman D., Ault R. (2017) Stratigraphy of the Roraima Supergroup along the Brazil-Guyana border in the Guiana shield, Northern Amazonian Craton - Results of the Brazil-Guyana Geology and Geodiversity Mapping Project. *Brazilian Journal of Geology*, Vol. 47, No. 1, pp. 43–57, https://doi.org/10.1590/2317-4889201720160139
Renfro N. (2015) The application of differential interference contrast microscopy to gemmology. *Journal of Gemmology*, Vol. 34, No. 7, pp. 616–620.
Ruiz-Agudo E., Putnis C.V., Jiménez-López C., Rodriguez-Navarro C. (2009) An atomic force microscopy study of calcite dissolution in saline solutions: The role of magnesium ions. *Geochimica et Cosmochimica Acta*, Vol. 73, No. 11, pp. 3201–3217, https://doi.org/10.1016/j.gca.2009.03.016
Santos J.O.S., Potter P.E., Reis N.J., Hartmann L.A., Fletcher I.R., McNaughton N.J. (2003) Age, source, and regional stratigraphy of the Roraima Supergroup and Roraima-like outliers in northern South America based on U-Pb geochronology. *Geological Society of America Bulletin*, Vol. 115, No. 3, pp. 331–348, https://doi.org/10.1130/0016-7606(2003)115%3C0331:ASARSO%3E2.0.CO;2
Schulze D.J., Nasdala L. (2016) Unusual paired pattern of radiohaloes on a diamond crystal from Guaniamo (Venezuela). *Lithos*, Vol. 265, pp. 177–181, https://doi.org/10.1016/j.lithos.2016.09.024
Smit K.V., Myagkaya E., Persaud S., Wang W. (2018) Black diamonds from Marange (Zimbabwe): A result of natural irradiation and graphite inclusions. *G&G*, Vol. 54, No. 2, pp. 132–148, https://doi.org/10.5741/GEMS.54.2.132
Smit K.V., Shirey S.B. (2020) Diamonds from the Deep: Diamonds are not forever! Diamond dissolution. *G&G*, Vol. 56, No. 1, pp. 148–155.
Stephan M., Bassoo R., Combs L. (2022) Lab Notes: The grass is always greener…. *G&G*, Vol. 58, No. 2, pp. 217–218.
Tappert R., Tappert M.C. (2011) *Diamonds in Nature: A Guide to Rough Diamonds*. Springer-Verlag, Berlin and Heidelberg.
Vance E.R., Milledge H.J. (1972) Natural and laboratory α-particle irradiation of diamond. *Mineralogical Magazine*, Vol. 38, No. 299, pp. 878–881, https://doi.org/10.1180/minmag.1972.038.299.11
Vance E.R., Harris J.W., Milledge H.J. (1973) Possible origins of α-damage in diamonds from kimberlite and alluvial sources. *Mineralogical Magazine*, Vol. 39, No. 303, pp. 349–360, https://doi.org/10.1180/minmag.1973.039.303.12
Vasilev E.A., Kozlov A.V., Petrovskii V.A. (2018) Volume and surface distribution of radiation defect in natural diamonds. *Journal of Mining Institute*, Vol. 230, pp. 107–115, https://doi.org/10.25515/pmi.2018.2.107
Wilks E., Wilks J. (1994) *Properties and Applications of Diamond*. Butterworth Heinemann Ltd., London.